Article

Video-based pooled screening yields improved far-red genetically encoded voltage indicators

In the format provided by the
authors and unedited

Contents

REAGENT or RESOURCE	SOURCE	IDENTIFIER
Bacterial and Virus Strains		
AAV2/9.hSyn::Cre.WPRE	UPenn Vector Core	N/A
AAV2/9.hSyn::DiO:SomQuasAr6a-EGFP.WPRE	In house	N/A
AAV2/9.hSyn::DiO:SomQuasAr6b-EGFP.WPRE	In house	N/A
AAV2/9.hSyn::DiO:SomQuasAr6a-EGFP-P2A-somCheRiff-HA.WPRE	Janelia Viral Tools	N/A
AAV2/9.hSyn::DiO:SomQuasAr6b-EGFP-P2A-somCheRiff-HA.WPRE	Janelia Viral Tools	N/A
AAV2/9.hSyn::DiO:SomArchon1-EGFP-P2A-somCheRiff-HA.WPRE	Janelia Viral Tools	N/A
Chemicals, Peptides, and Recombinant Proteins		
doxycycline hyclate	Sigma	Cat# D9891
Blasticidin S	Sigma	Cat# 203350
Puromycin dihydrochloride from *Streptomyces alboniger*	Sigma-Aldrich	Cat# P7255
Geneticin® Selective Antibiotic (G418 Sulfate)	ThermoFisher	Cat# 11811023
HA Tag recombinant rabbit monoclonal antibody	ThermoFisher	Cat# RM305
goat anti-Rabbit IgG (H+L) cross-adsorbed secondary antibody conjugated with Cy-5	ThermoFisher	
Experimental Models: Cell Lines		
HEK293T	ATCC	ATCC CRL-3216
tet-on spiking HEK cell	This work	ATCC CRL-3479
CheRiff-EGFP tet-on spiking HEK cell	This work	ATCC CRL-3480
CheRiff-CFP tet-on spiking HEK cell	This work	N/A
Experimental Models: Organisms/Strains		
C57BL/6 wild-type mice	Charles River	Strain Code 027

NDNF-Cre transgenic mice	Jackson Lab	Stock #028536
PV-Cre transgenic mice	Catherine Dulac	Stock #017320
Recombinant DNA constructs		
TDG004 pLenti_CMVtight_Kir2.1-CFP	This work	Addgene #178820
pLenti-CMV-rtTA3-Blast	Eric Campeau	Addgene #26429
HT028 FCMV_CheRiff-EGFP	This work	Addgene #178821
HT041 FCMV_CheRiff-CFP	This work	Addgene #136636
HT063 FCMV_Archon1-Citrine	This work	
HT075 Fsyn_FAS(Cre-off) Archon1-Citrine	This work	
HT091 FCMV_Archon1-dark citrine_P2A_mEos4a	This work	
HT103 FCMV_QuasAr6a-Citrine	This work	Addgene #178822
HT110 FCMV_QuasAr6b-Citrine	This work	Addgene #178823
HT111 Fsyn_FAS(Cre off)_QuasAr6a-Citrine	This work	Addgene #178824
HT114 Fsyn_FAS(Cre-off)_QuasAr6b-Citrine	This work	Addgene #178825
HT107 pAAV_hSyn-DiO-SomQuasAr6a_EGFP-P2A-somCheRiff_HA	This work	Addgene #178826
HT109 pAAV_hSyn-DiO-SomQuasAr6a_EGFP	This work	Addgene # 190878
HT115 pAAV_hSyn-DiO-SomQuasAr6b_EGFP-P2A-somCheRiff_HA	This work	Addgene #178827
HT116 pAAV_hSyn-DiO-SomQuasAr6a_EGFP	This work	Addgene # 190879
Software and Algorithms		
MATLAB R2016b - 2020a	Mathworks	Matlab
Labview 2014, 2015	National Instruments	Labview
FCS Express 7 Research	De Novo Software	FCS Express
NoRMCorre	[1]	https://github.com /flatironinstitute/NoRMCorre

Others		
Custom-designed ultra-widefield microscope	2	N/A
Custom-designed structured illumination microscope	3	N/A

Supplementary Table 1. List of reagents and materials

	Cell type	Constructs tested	Set-up	Metrics	Related Figures
In vitro	HEK293T cells	1.QuasAr6a-Citrine 2.QuasAr6b-Citrine 3.Archon1-Citrine	High-magnification, widefield inverted microscope + electrophysiology	per-molecule brightness; voltage sensitivity (F-V); kinetics; photostability; non-linear photophysics	Extended Data Fig.4b-f Supplementary Figure 3g
In vitro	HEK293T cells	1.QuasAr6a-Citrine 2.QuasAr6b-Citrine	High-magnification, widefield inverted microscope + electrophysiology	trafficking; photocurrent	Extended Data Fig.4a,g,h
In vitro	Rat hippocampal neurons	1.QuasAr6a-Citrine 2.QuasAr6b-Citrine	Confocal microscope	trafficking	Fig.3b
In vitro	Rat hippocampal neurons	1.QuasAr6a-Citrine 2.QuasAr6b-Citrine	High-magnification, widefield inverted microscope + electrophysiology	voltage sensitivity (F-V);	Fig.3c
In vitro	Rat hippocampal neurons	1.QuasAr6a-Citrine 2. QuasAr6b-Citrine 3. Archon1-Citrine 4. Archon1-EGFP (co-expression with CheRiff-CFP)	low-magnification, widefield inverted microscope	SNR; optical spike width; voltage sensitivity ($\Delta F/F_0$ per spike); expression level; brightness; per-molecule brightness	Fig.3d-j; Extended Data Fig.5
Ex vivo	Mouse cortical and hippocampal PV neurons, fixed slice	1. somQuasAr6a-P2A- somCheRiff_HA 2. somQuasAr6b-P2A-somCheRiff_HA	Confocal microscope	expression and trafficking	Extended Data Fig.6
Ex vivo	Mouse cortical neurons in acute slice	1.somQuasAr6a-EGFP 2.somQuasAr6b-EGFP	High-magnification, widefield upright microscope + electrophysiology	impact on cell electrophysiological properties; optical spike waveform; non-linear photophysics;	Fig.3k-p; Extended Data Fig.7; Supplementary Figure 3g
In vivo	Mouse cortex, NDNF+ neurons	1.somQuasAr6a-P2A-somCheRiff_HA 2. somQuasAr6b-P2A-somCheRiff_HA 3. somArchon1-P2A-somCheRiff_HA	Structured illumination upright microscope	SNR; optical spike widths; optical spike waveform; photostability	Fig.4a-e; Extended Data Fig.9
In vivo	Mouse hippocampus CA1, PV+ neurons	1.somQuasAr6b-P2A-somCheRiff_HA 2.somArchon1-P2A-somCheRiff-HA	Structured illumination upright microscope	SNR; optical spike widths; optical spike waveform; photostability	Fig.4f-l; Extended Data Fig.8,9

Supplementary Table 2. Summary of the experiments characterizing QuasAr6a and QuasAr6b.
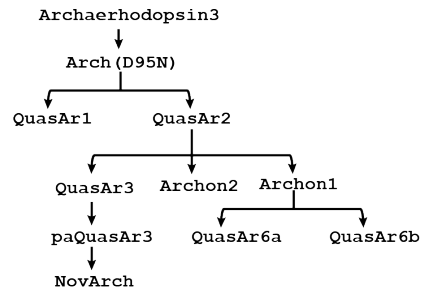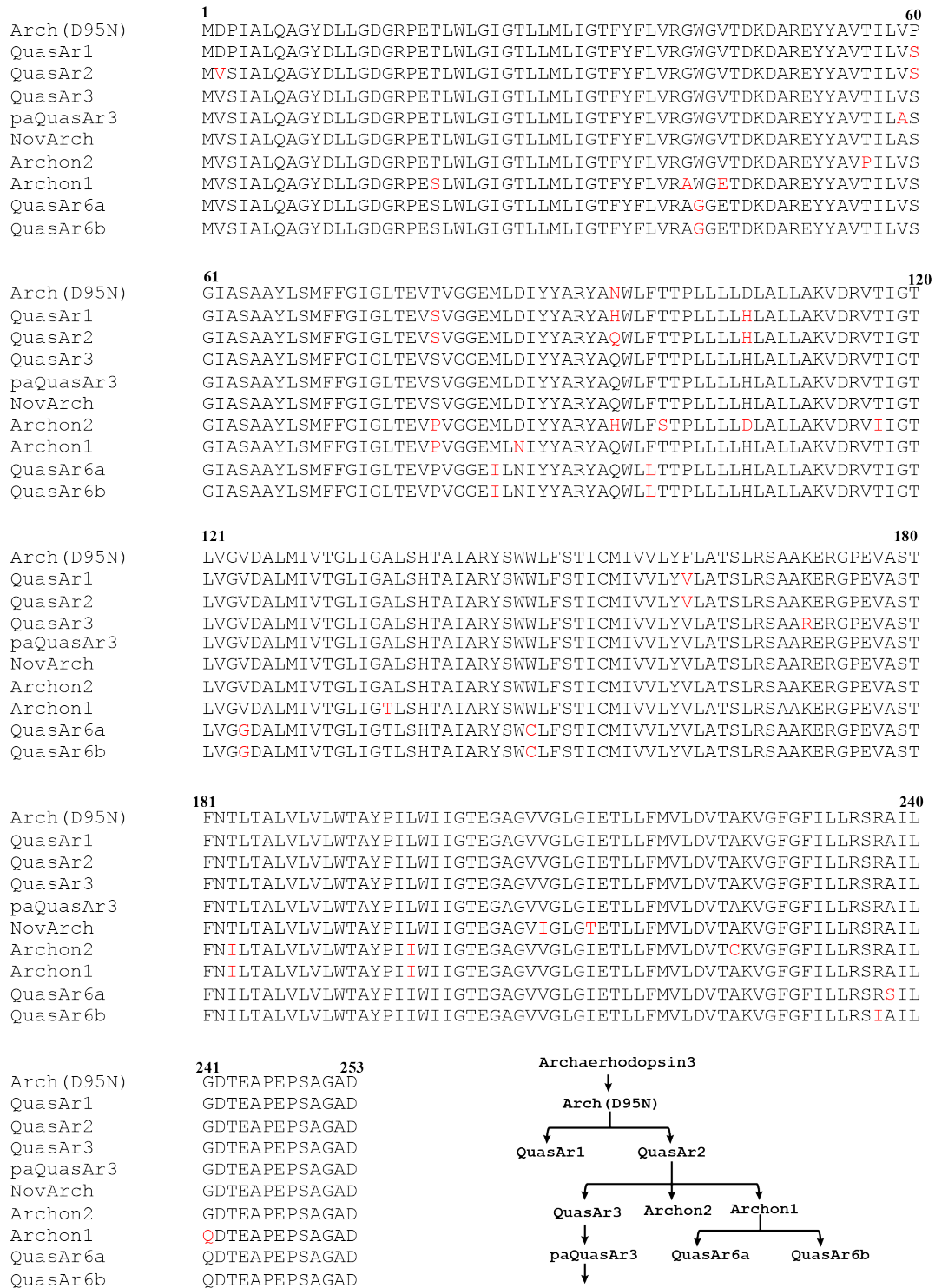
Cell type	Related Figures	Objective	Patterning	Intensity (Exc. 635; mW)	Frame rate (Hz)
NDNF	Fig. 4a-e	25x	Membrane-focal	5	996
NDNF	Fig. 5	25x	Soma-targeted	3~4	996
PV	Extended Data Fig.9	25x	Soma-targeted	4	996
PV	Fig. 4f-i	25x	Membrane-focal	10	1973
PV	Extended Data Fig. 8	10x	Soma-targeted	10	1973
PV	Extended Data Fig. 8	10x	Membrane-focal	10	3947
PV	Fig. 6	10x	Soma-targeted	7~8	1973
PV	Extended Data Fig.9	25x	Soma-targeted	8	1973

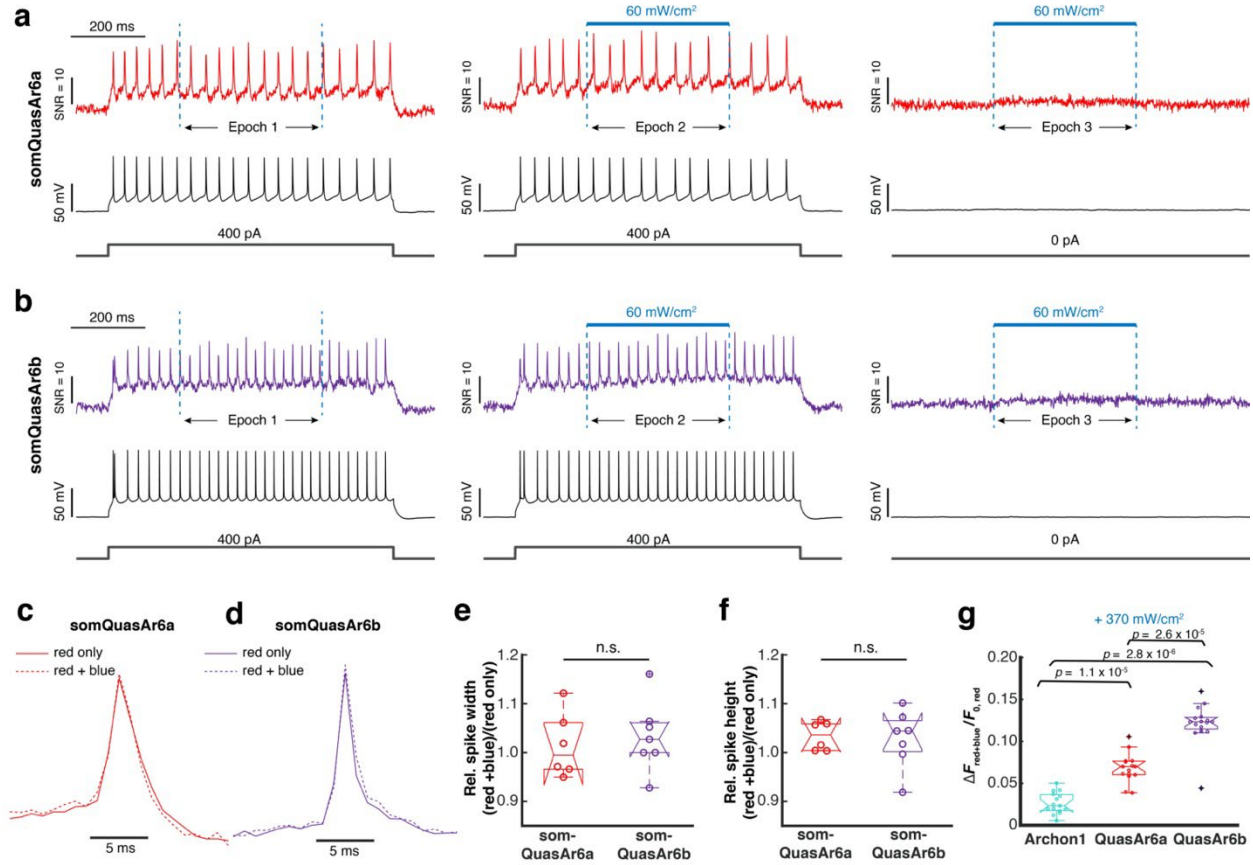**Supplementary Table 3. Summary of the conditions for *in vivo* imaging**
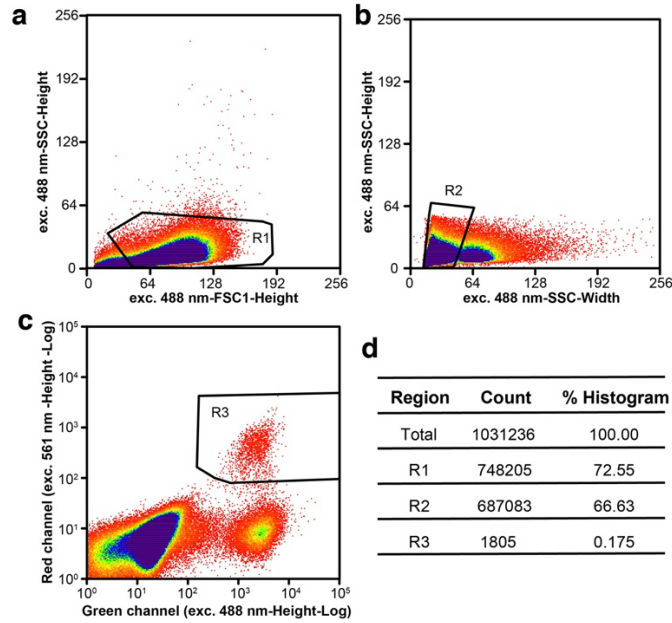
Supplementary Figure 1. The FACS gating strategy to isolate the phototagged library cells.
FSC: forward Scatter. SSC: side-scatter. After removal of cell debris (**a**), cells within R1 were
further purified to remove doublet cells (**b**). Cells within R2 were selected based on the green
channel (exc.488 nm) and red channel (exc.561 nm) signal (**c**). The double-positive cells within
in R3 were collected and cultured. **d**. Statistics for each Region of Interest.

```
                1                                                          60
Arch(D95N)      MDPIALQAGYDLLGDGRPETLWLGIGTLLMLIGTFYFLVRGWGVTDKDAREYYAVTILVP
QuasAr1         MDPIALQAGYDLLGDGRPETLWLGIGTLLMLIGTFYFLVRGWGVTDKDAREYYAVTILVS
QuasAr2         MVSIALQAGYDLLGDGRPETLWLGIGTLLMLIGTFYFLVRGWGVTDKDAREYYAVTILVS
QuasAr3         MVSIALQAGYDLLGDGRPETLWLGIGTLLMLIGTFYFLVRGWGVTDKDAREYYAVTILVS
paQuasAr3       MVSIALQAGYDLLGDGRPETLWLGIGTLLMLIGTFYFLVRGWGVTDKDAREYYAVTILAS
NovArch         MVSIALQAGYDLLGDGRPETLWLGIGTLLMLIGTFYFLVRGWGVTDKDAREYYAVTILAS
Archon2         MVSIALQAGYDLLGDGRPETLWLGIGTLLMLIGTFYFLVRGWGVTDKDAREYYAVPILVS
Archon1         MVSIALQAGYDLLGDGRPESLWLGIGTLLMLIGTFYFLVRAWGETDKDAREYYAVTILVS
QuasAr6a        MVSIALQAGYDLLGDGRPESLWLGIGTLLMLIGTFYFLVRAGGETDKDAREYYAVTILVS
QuasAr6b        MVSIALQAGYDLLGDGRPESLWLGIGTLLMLIGTFYFLVRAGGETDKDAREYYAVTILVS


                61                                                         120
Arch(D95N)      GIASAAYLSMFFGIGLTEVTVGGEMLDIYYARYANWLFTTPLLLLDLALLAKVDRVTIGT
QuasAr1         GIASAAYLSMFFGIGLTEVSVGGEMLDIYYARYAHWLFTTPLLLLHLALLAKVDRVTIGT
QuasAr2         GIASAAYLSMFFGIGLTEVSVGGEMLDIYYARYAQWLFTTPLLLLHLALLAKVDRVTIGT
QuasAr3         GIASAAYLSMFFGIGLTEVSVGGEMLDIYYARYAQWLFTTPLLLLHLALLAKVDRVTIGT
paQuasAr3       GIASAAYLSMFFGIGLTEVSVGGEMLDIYYARYAQWLFTTPLLLLHLALLAKVDRVTIGT
NovArch         GIASAAYLSMFFGIGLTEVSVGGEMLDIYYARYAQWLFTTPLLLLHLALLAKVDRVTIGT
Archon2         GIASAAYLSMFFGIGLTEVPVGGEMLDIYYARYAHWLFSTPLLLLDLALLAKVDRVIIGT
Archon1         GIASAAYLSMFFGIGLTEVPVGGEMLNIYYARYAQWLFTTPLLLLHLALLAKVDRVTIGT
QuasAr6a        GIASAAYLSMFFGIGLTEVPVGGEILNIYYARYAQWLLTTPLLLLHLALLAKVDRVTIGT
QuasAr6b        GIASAAYLSMFFGIGLTEVPVGGEILNIYYARYAQWLLTTPLLLLHLALLAKVDRVTIGT


                121                                                        180
Arch(D95N)      LVGVDALMIVTGLIGALSHTAIARYSWWLFSTICMIVVLYFLATSLRSAAKERGPEVAST
QuasAr1         LVGVDALMIVTGLIGALSHTAIARYSWWLFSTICMIVVLYVLATSLRSAAKERGPEVAST
QuasAr2         LVGVDALMIVTGLIGALSHTAIARYSWWLFSTICMIVVLYVLATSLRSAAKERGPEVAST
QuasAr3         LVGVDALMIVTGLIGALSHTAIARYSWWLFSTICMIVVLYVLATSLRSAARERGPEVAST
paQuasAr3       LVGVDALMIVTGLIGALSHTAIARYSWWLFSTICMIVVLYVLATSLRSAARERGPEVAST
NovArch         LVGVDALMIVTGLIGALSHTAIARYSWWLFSTICMIVVLYVLATSLRSAAKERGPEVAST
Archon2         LVGVDALMIVTGLIGALSHTAIARYSWWLFSTICMIVVLYVLATSLRSAAKERGPEVAST
Archon1         LVGVDALMIVTGLIGTLSHTAIARYSWWLFSTICMIVVLYVLATSLRSAAKERGPEVAST
QuasAr6a        LVGGDALMIVTGLIGTLSHTAIARYSWCLFSTICMIVVLYVLATSLRSAAKERGPEVAST
QuasAr6b        LVGGDALMIVTGLIGTLSHTAIARYSWCLFSTICMIVVLYVLATSLRSAAKERGPEVAST


                181                                                        240
Arch(D95N)      FNTLTALVLVLWTAYPILWIIGTEGAGVVGLGIETLLFMVLDVTAKVGFGFILLRSRAIL
QuasAr1         FNTLTALVLVLWTAYPILWIIGTEGAGVVGLGIETLLFMVLDVTAKVGFGFILLRSRAIL
QuasAr2         FNTLTALVLVLWTAYPILWIIGTEGAGVVGLGIETLLFMVLDVTAKVGFGFILLRSRAIL
QuasAr3         FNTLTALVLVLWTAYPILWIIGTEGAGVVGLGIETLLFMVLDVTAKVGFGFILLRSRAIL
paQuasAr3       FNTLTALVLVLWTAYPILWIIGTEGAGVVGLGIETLLFMVLDVTAKVGFGFILLRSRAIL
NovArch         FNTLTALVLVLWTAYPILWIIGTEGAGVIGLGTETLLFMVLDVTAKVGFGFILLRSRAIL
Archon2         FNILTALVLVLWTAYPIIWIIGTEGAGVVGLGIETLLFMVLDVTCKVGFGFILLRSRAIL
Archon1         FNILTALVLVLWTAYPIIWIIGTEGAGVVGLGIETLLFMVLDVTAKVGFGFILLRSRAIL
QuasAr6a        FNILTALVLVLWTAYPIIWIIGTEGAGVVGLGIETLLFMVLDVTAKVGFGFILLRSRSIL
QuasAr6b        FNILTALVLVLWTAYPIIWIIGTEGAGVVGLGIETLLFMVLDVTAKVGFGFILLRSIAIL


                241      253
Arch(D95N)      GDTEAPEPSAGAD
QuasAr1         GDTEAPEPSAGAD
QuasAr2         GDTEAPEPSAGAD
QuasAr3         GDTEAPEPSAGAD
paQuasAr3       GDTEAPEPSAGAD
NovArch         GDTEAPEPSAGAD
Archon2         GDTEAPEPSAGAD
Archon1         QDTEAPEPSAGAD
QuasAr6a        QDTEAPEPSAGAD
QuasAr6b        QDTEAPEPSAGAD
```


Supplementary Figure 2. Alignment of the amino acid sequences of representative Arch-based GEVIs. Lower right: lineage tree indicating the historical development of different GEVIs. The amino acid substitutions that distinguish each GEVI from its parent are highlighted in red.

Supplementary Figure 3. Effect of blue light on far-red optical spike waveform. Concurrent fluorescence and voltage recordings were performed for mouse L2/3 cortical neurons expressing somQuasAr6a-EGFP or somQuasAr6b-EGFP in acute slice. **a, b**. Example fluorescence traces with and without the blue light. Spikes were evoked via current injection. The blue light intensity (exc. 488 nm, 60 mW/cm^2) was within the range needed for optogenetic activation. To control for spike waveform adaptation during steady current injection, only the spikes from Epoch 1 (red-only) and Epoch 2 (red + blue) were used to calculate the average fluorescence waveforms. The fluorescence traces in Epoch 3 showed that blue light crosstalk was negligible under these conditions. **c, d**. Spike-triggered average fluorescence waveforms calculated from the traces shown in **a**, **b**. **e**. Relative optical spike widths ((red + blue)/(red-only)) of somQuasAr6a-expressing neurons (mean ± S.D., 1.01 ± 0.07, *n* = 6 cells) and somQuasAr6b-expressing neurons (mean ± S.D., 1.03 ± 0.08, *n* = 7 cells). n.s., not significant (Wilcoxon rank-sum test). **f**. Relative optical spike heights ((red + blue)/(red-only)) of somQuasAr6a-expressing neurons (mean ± S.D., 1.03 ± 0.03; *n* = 6 cells) and somQuasAr6b-expressing neurons (mean ± S.D., 1.03 ± 0.06, *n* = 7 cells). n.s., not significant (Wilcoxon rank-sum test). **g**. Quantification of blue-light induced photoactivation (635 nm, 420 W/cm^2; 488 nm, 0.37 W/cm^2) in HEK cells. The blue-

activation coefficient is defined as the Arch-channel fluorescence signal change under both blue and red excitation ($F_{ex488+ex635}$ - F_{ex488} - F_{ex635}), normalized by the baseline Arch-channel fluorescence ($F_{0, ex635}$) [4]. Blue-activation coefficient (mean ± S.D.): 0.02 ± 0.01 for Archon1 (n = 15 cells); 0.07 ± 0.02 for QuasAr6a (n = 15 cells); 0.12 ± 0.02 for QuasAr6b (n = 16 cells), two-sided Wilcoxon rank-sum test. Box plots: central mark indicates median, bottom edge 25th percentile, top edge 75th percentile, whiskers most extreme data points excluding outliers, '+' symbol outliers.

SUPPLEMENTARY METHODS

Molecular cloning

Restriction endonucleases were purchased from New England BioLabs (NEB). Non-mutagenic PCR reactions were performed with Phusion® High-Fidelity DNA Polymerase (NEB, Cat. # M0530L). Synthetic DNA oligonucleotides used for cloning were purchased from Integrated DNA Technologies (IDT). Opsin sequences containing a single point mutation were generated through site-directed mutagenesis (QuikChange Lightning Single or Multi kit, Agilent Technologies, Part # 210518 or 210519). Opsin sequences containing multiple point mutations were synthesized *de novo* as gBlocks (IDT). Error-prone PCR was performed with GeneMorph II Random Mutagenesis Kits (Agilent Technologies, Part # 200552) or home-made PCR cocktail (NEB Taq polymerase, 5 mM $MgCl_2$, 0.2 mM each of dGTP and dATP, and 1.0 mM each of dCTP and dTTP). Small-scale isolation of plasmid DNA was performed in house with GeneJET miniprep kit (Thermo Scientific, Cat.# K0503). Large-scale isolation of plasmid DNA was outsourced to Genewiz. The design of the soma-targeted QuasAr6a and QuasAr6b AAV was similar to that of somArchon1. [5] The design of the cre-on bicistronic Optopatch construct of QuasAr6b and QuasAr6b (pAAV_hSyn-DiO-SomQuasAr6-EGFP-P2A-somCheRiff_HA) was based on Optopatch4 that used Archon1 as the voltage indicator [3].

HEK cell culture

Wild-type or engineered HEK293T cell lines were maintained at 37 °C, 5% CO_2 in Dulbecco's Modified Eagle Medium (DMEM) supplemented with 10% fetal bovine serum, 1% GlutaMax-I, penicillin (100 U/mL), streptomycin (100 mg/mL). For maintaining or expanding the cell culture, we used TC-treated culture dish (Corning). For all the imaging experiments, cells were plated on glass-bottomed dish dishes (Cellvis, Cat.# D35-14-1.5-N). Before optical stimulation and imaging, the medium was replaced with extracellular (XC) buffer containing 125 mM NaCl, 2.5 mM KCl, 3 mM $CaCl_2$, 1 mM $MgCl_2$, 15 mM HEPES, 30 mM glucose (pH 7.3). We found that the XC buffer maintained the cell adhesion and response to optogenetic stimulation for at least 7 - 8 hours.

Lentivirus packaging

All the lentivirus preparations were made in house. HEK293T cells were co-transfected with the second-generation packaging plasmid psPAX2 (Addgene #12260), envelope plasmid VSV-G (Addgene #12259) and transfer plasmids at a ratio of 9:4:14. In this study, we generally used FCMV, sometimes pLenti-CMV, as the transfer vector for HEK cell experiments. We used FSyn for cultured neuron experiments [6]. Both FCMV and FSyn were modified from a previously

described FCK lentivirus vector [7] by replacing the original CaMKII with a CMV or a hSyn promoter, respectively. For lentivirus intended for HEK cell transduction, 2.7 μg total plasmids for a small culture (300k cells in 35-mm dish) gave sufficient yield of lentivirus. For cultured neuron transduction, larger cultures in 15-cm dish or 10-layer HYPER Flasks (CheRiff construct, Corning #10030) were used, and HEK cells were transfected with PEI using established protocols [8]. The harvested vrus was concentrated 10-fold (voltage sensors) or 30-fold (CheRiff) using a cationic polymer (Takara Lenti-X Concentrator).

In-house AAV packaging

AAV2/9 hSyn-DiO-SomQuasAr6a-EGFP and AAV2/9 hSyn-DiO-SomQuasAr6b-EGFP were packaged in house based on a published protocol [9]. Briefly, 50~70% confluent HEK293T cells grown in DMEM supplemented with 5% FBS were triple transfected with pHelper, pAAV ITR-expression, and pAAV Rep-Cap plasmids using acidified PEI (DNA-to-PEI ratio = 1: 3) in 1~2 T175 flasks (~ 2 x 10^7 cells each flask). The AAV-containing medium was harvested on Day 3, and the AAV-containing medium and cells were harvested on Day 5. For the second cell-containing harvest, AAVs were released from the cells with citrate buffer (55 mM citric acid, 55 mM sodium citrate, 800 mM NaCl, 3 mL per flask). The two harvests were then combined and precipitated with PEG/NaCl (5x, 40% PEG 8000 (w/v), 2.5 M NaCl, 4°C overnight). The low-titer virus was then purified with chloroform extraction (viral suspension and chloroform 1:1 (v/v)), aqueous two-phase partitioning (per 1 g of the AAV-containing supernatant, add 5 g of 20% (NH4)2SO4 solution and 1.5 g of 50% PEG 8000 solution, and iodixanol discontinuous gradient centrifugation (15%, 25%, 40%, and 54% iodixanol gradient prepared from OptiPrep (60% (w/v) Iodixanol, Axis-Shield PoC AS). The purified AAV was tittered with qPCR (SYBR Green, primer for forward ITR: 5'-GGAACCCCTAGTGATGGAGTT-3'; primer for reverse ITR sequence 5'-CGGCCTCAGTGAGCGA-3').

Engineering monoclonal spiking HEKs

All the spiking HEK cells were engineered on HEK293T background (ATCC CRL-3216). First, $Na_V1.5$-Puro^{+} HEK293T cells were generated as previously described [10]. The tet-inducible expression system was designed by the Eric Campeau lab and obtained through Addgene. $K_{ir}2.1$-CFP was cloned into the open reading frame of pLenti-CMVtight-EGFP-Neo vector (Addgene Plasmid #26586). pLenti-CMV-rtTA3-Blast (Addgene Plasmid #26429) was used directly to package lentivirus. $Na_V1.5$-Puro+ HEK293T cells were simultaneously infected with pLenti-CMV-rtTA3-Blast and pLenti-CMVtight-$K_{ir}2.1$-CFP-Neo (TDG004). The cells were first selected with three antibiotics (2 μg/mL puromycin, 5 μg/mL blasticidin, 200 μg/mL Geneticin/G418), then

induced with doxycycline (2 µg/mL) for ~30 hours before FACS purification. The CFP+ cells were seeded into 96-well plates (1 cell per well) and cultured 3 - 4 weeks under the standard conditions for HEK cell culture. The expanded monoclonal cells were screened with current clamp. The clone that showed robust spike upon current injection was termed tet-on spiking HEK cell and used to engineer the CheRiff-CFP+ spiking HEK cells.

CheRiff-CFP was cloned into FCMV lentivirus vector (HT041). After lentiviral infection and monoclonal selection, the CheRiff-CFP+ spiking HEK cells were optically screened. The spikes were evoked with optogenetic stimulation (exc. 490 nm) and visualized using a voltage-sensitive dye (BeRST, exc. 635 nm) [11]. The CheRiff-EGFP+ spiking HEK cells were engineered differently. Nav1.5-Puro/rtTA3-Blast/K_{ir}2.1-CFP-Neo+ polyclonal HEK cells were infected with FCMV-CheRiff-EGFP (HT028) lentivirus. After doxycycline induction, the CFP+/EGFP+ cells were purified by FACS and seeded into 96-well plate for monoclonal selection. The monoclonal cells were validated by patch clamp under optogenetic stimulation.

To enhance genomic stability, the spiking HEK cells can be maintained in antibiotic-containing medium (2 µg/mL puromycin, 5 µg/mL blasticidin, 200 µg/mL Geneticin/G418). However, we found the cell lines reasonably stable even without these antibiotics. To obtain consistent experimental results, we only used low passage-number cells and kept a master plate free of doxycycline.

Tet-on spiking HEK cell and CheRiff-EGFP+ tet-on spiking HEK cell are available from ATCC (CRL-3479; CRL-3480).

Photoselection system

Optical system

The optical system was described in an earlier publication [2] with a few modifications for the present use. The microscope was in an inverted configuration to facilitate imaging of cultured cells in glass-bottomed dishes. The system was equipped with several light sources delivered to the sample through free-space optics: 1) a 635-nm laser (DILAS 8 Watts, MB-638.3-8C-T25-SS4.3) sent to the sample plane from below through a near-total internal reflection (near-TIR) configuration for imaging archaerhodopsin-derived GEVIs; 2) LEDs mounted from the above for optogenetic stimulation and imaging fluorescent proteins; 3) a 405-nm laser (MDL-W-405-1W) projected to a micromirror-array device (Digital light innovations, Discovery D4100 with DLP9500 chip and ALP 4.1 High-Speed control software) for photoselection. The patterned light was collected with a tube lens (Olympus MVX, 0.63×) and directed to the sample by a small 45° mirror

(4 mm mirror, Tower Optical, MPCH-4.0) inserted into the infinity space. The emission fluorescence was collected with a low-magnification (2×) and high-numerical aperture (NA 0.5) objective lens and filtered with wavelength-specific filters inserted into the infinity space. The emission filter wheel was tilted by a small angle to avoid reflection of light between the sample dishes and filters. After filtering, the emission light was reimaged through a tube lens (Zeiss, Milvus 2/135) and recorded with a scientific CMOS camera (Hamamatsu, ORCA-Flash 4.0). The system was controlled by custom-made LabView codes.

Calibration of patterned illumination

We used a digital micromirror array device (DMD) to illuminate target cells, and calibrated it for precise optical targeting of single cells over a large field of view (2.3 mm × 2.3 mm, Extended Data Fig. 1a).   The DMD comprised a 1920 ×1080 array, which did not provide 1:1 correspondence with the camera chip (1024×1024 at binning = 2). Moreover, small alignment errors and optical aberrations could manifest as substantial projection errors. To register the DMD array with the camera pixel coordinates, we projected an equally spaced (d = 50 pixels), 11×11 array of dots (20 pixels interval) onto a fluorescent exposure target (exc. 405-nm; CFP emission filter). The dimension of this test pattern (500 × 500 pixels) was intended to cover the field of view (FOV) for GEVI screening. The center of each dot in the camera image was determined by 2D Gaussian fitting of the point-spread function. The transformation relationship between actual projection and the expected projection was determined using Matlab Image Processing Toolbox (imwarp, piecewise linear transformation).

Comparison of different phototaggable FPs

We evaluated three candidate phototaggable FPs for Photopick (Extended Data Fig. 1b): mEos4a, a green-to-red photoconvertible FP [12]; PA-mCherry, a red photoactivable FP [13], and PA-GFP, a green photoactivable FP [14]. Phototransformation was most efficient for mEos4a (fluence at 405 nm for 50% phototagging: 5.4 ± 0.3 J/cm^2 for mEos4a; 18 ± 4 J/cm^2 for PA-mCherry; 140 J/cm^2 for PA-GFP, Extended Data Fig. 1c), and mEOS4a had a spectral window compatible with Arch-derived GEVIs, so we selected this protein as our photo-tag.

Calibration of selection efficiency and fidelity

We evaluated the efficiency and fidelity of Photopick. We plated a mixture of mEos4a$^+$ cells (green-to-red), PA-mCherry$^+$ cells (dark-to-red) and blank HEK cells (approximate final ratio 1:2:50) in a monolayer on the glass-bottomed dish (Fig. 1b). The ratios of cell numbers were selected to approximate the conditions in subsequent experiments. We sought to photoconvert

the mEos4a$^+$ cells while not converting the PA-mCherry$^+$ cells. We imaged the green (mEos4a) fluorescence and then applied patterned illumination of violet light targeted to the mEos4a$^+$ pixels (Fig. 1c). FACS analysis showed that the fidelity (phototagged mEos4a$^+$ cells/(phototagged mEos4$^+$ cells + phototagged PA-mCherry$^+$ cells)) was approximately 96% and efficiency (phototagged mEos4a$^+$ cells/all mEos4$^+$ cells) was approximately 85% (Fig. 1d; see also Extended Data Fig. 1d.). We concluded that the Photopick system had sufficient precision for phenotype-activated photoselection at cellular resolution.

Video-based pooled screening for engineering improved GEVIs

Generation of the library cells

Archon1 sequence was a gift from Ed Boyden at MIT. Previously, we found that a fluorescent protein tag could significantly enhance the membrane localization of Archaerhodopsin-derived GEVIs in mammalian cells. In particular, a combination of Citrine and multiple repeats of trafficking sequence (TS-Citrine-TS×3-ER2) improved the voltage imaging SNRs in cultured neuron [15]. Initially, we attempted to substitute Citrine with mEos4a. However, this substitution resulted in poorly trafficked protein. Therefore, we switched to a bicistronic construct, in which GEVI and mEos4a were linked with a self-cleaving P2A peptide [16]. Because Citrine and mEos4a share the same spectral window, a single point mutation (Y67G) was introduced into Citrine to create a non-fluorescent protein tag, "dark Citrine" [6].

Random mutations were introduced into Archon1 using error-prone PCR. Then the mutated opsin sequences were fused to the rest of the coding sequence (TS-dark Citrine-TS×3-ER2-P2A-mEos4a) using fusion PCR and purified with agarose gel electrophoresis. The purified DNA fragment was inserted into the FCMV lentivirus vector using Gibson assembly, transformed into DH5α *E*. coli competent cells (NEB), and plated on ampicillin-containing (Amp+) agar plates. We used Sanger sequencing to analyze the mutation rate of a small number (<10) of clones. Each mutant included 0, 1, or 2 amino acid substitutions (average number ~ 1). The colonies were scraped from the agar plates, transferred into Amp+ LB medium, allowed to grow at room temperature for approximately 1 hour before miniprep. The plasmid library was then used for lentivirus preparation. CheRiff-CFP$^+$ spiking HEK cells were infected with the lentivirus library at a low titer (MOI ~ 0.01). The mEos4a$^+$ cells were purified with FACS and cultured with the standard HEK cell culture protocol. In this study, we generated two random mutagenesis libraries based on Archon1. Each was independently evolved and analyzed on the Photopick platform.

Image segmentation and ROI selection

The 500 × 500-pixel FOV (2.3 mm × 2.3 mm in the sample plane) was segmented based on the mEOS-channel (excited with 490-nm LED) image using custom Matlab code. Briefly, the mEos4a-channel image was corrected for baseline and segmented with Watershed algorithm. Only ROIs larger than 5 pixels were accepted as "cells", and smaller ROIs were rejected. We observed that after 2 days of culture, the library cells often showed small clusters, primarily due to cell division. We reasoned that since the neighboring cells descended from the same parent cells, it was acceptable to treat small clusters as a single genotype.

In pilot experiment in Extended Data Fig. 2c, the library cells were replaced with the monoclonal CheRiff+/Archon1-Citrine+ spiking HEK cells. We found that even a monoclonal population showed substantial variation in F_0 and ΔF, possibly due to variations in protein expression or trafficking. Thus, we concluded that 1) there were non-genetic factors underlying the broad distribution of expression level, and 2) setting a stringent threshold for F_0 was unlikely to be meaningful. In our experiments, we set a 50th percentile threshold for $F_{0,Arch}$, and 75th percentile cut-off for $\Delta F_{Arch}/\sqrt{F_{0,Arch}}$. These top 12.5% of ROIs were selectively illuminated with violet light to create a binary marker.

Fluorescence-activated cell sorting (FACS)

FACS was performed on a BD FACS Aria Cell Sorters. The gating strategy is shown in Supplementary Figure 1. The data was analyzed with FCSExpress 7 Research Edition.

Illumina sequencing

16k - 20k library cells were collected into PCR tubes and boiled (98 °C, 5 min) to release their genomes as the PCR template. The opsin sequences were amplified from the genome (forward primer: GACCTCCTCGGAGATGGTAGA; reverse primer: AGCTGAAGGTTCAGGTGCTTC). The primer pair used here gave a 720-bp amplicon that covered the 31-750 nt of Archon1 CDS, which effectively provided single nucleotide polymorphism (SNP) information for 52-729 nt. We also attempted primers designed to cover the entire 759 nt of Archon1 CDS. However, we found that full-coverage primers did not result in robust PCR amplification. We reasoned that as the N-terminus and C-terminus are distant from the retinal chromophore and unlikely to modulate the voltage-sensitive fluorescence, the omission of the terminal sequence information should not severely negatively impact our screening efforts. In the earlier efforts to optimize archaerhodopsin-derived GEVIs, no beneficial mutations have been identified in the missing regions [7, 17].

The 720-bp amplicon were then segmented into 3 smaller amplicons with high-fidelity PCR:

Fwd1:   TCGTCGGCAGCGTCAGATGTGTATAAGAGACAG-GACCTCCTCGGAGATGGTAG,

Rev1:   GTCTCGTGGGCTCGGAGATGTGTATAAGAGACAG-TGTAGTGAACAGCCACTGTG;

Fwd2:   TCGTCGGCAGCGTCAGATGTGTATAAGAGACAG-CTGAACATCTACTACGCAAG,

Rev2:   GTCTCGTGGGCTCGGAGATGTGTATAAGAGACAG-CTGGGCCTCTCTCCTTAGCG;

Fwd3:   TCGTCGGCAGCGTCAGATGTGTATAAGAGACAG-GTCCTGGCCACTTCTCTGCG;

Rev3: GTCTCGTGGGCTCGGAGATGTGTATAAGAGACAG-AGCTGAAGGTTCAGGTGC).

We chose 2 x 150 bp paired-end MiSeq (Harvard Medical School Biopolymer Facility) to analyze the SNPs. We obtained a sequencing depth of 2 - 5 ×10^5 reads per nt (filtered for Illumina Q score > 30). VCF data were generated from the FASTAQ data with a custom pipeline that included Trimomatic [18], NGmerge [19], BWA [20], samtools [21], and Pilon [22]. The VCF data were subsequently analyzed with custom Matlab code.

Simulation of the selection threshold

To determine the probability that a mutation could be enriched in the selection by chance alone, we performed a Matlab simulation of the selection process, assuming random selection for a mutant with starting frequencies of 0.002%, 0.004%, 0.006%, 0.008%, 0.01%, 0.02%, 0.03%, 0.04%, 0.05%, 0.06%,0.07, 0.08%. The upper limit of 0.08% was chosen based on the sequencing result of the starting library. The initial number of library cells was set to be 50,000. We randomly allowed 5,000 – 12,000 "cells" to pass the selection. These numbers were determined by the actual numbers of cells collected from FACS (5,000 ~12000 cells after each round). We then expanded the population 100-fold and repeated the sampling and expansion process two more times. The 95% confidence threshold on the prevalence of a mutational frequency arising by chance was determined from 2,000 iterations of the simulation.

High-throughput imaging of hippocampal neurons

Functional Optopatch imaging was performed after 14 days in culture on the Firefly microscope [8]. The Firefly microscope was fully automated and ran with no human intervention. Imaging was performed at room temperature and no extra heating was provided so as to reduce evaporation-related artifacts. The whole plate was scanned automatically with motorized stages so that the three FOVs within each well were evenly spaced. Focus was also automatically adjusted for each FOV. Optogenetic stimulus to CheRiff was generated by a blue LED, filtered (Semrock No. FF01-470/28), and delivered to a large area with intensity ranging from 2 to 88 mW/cm^2. 638 nm red laser light was applied through a prism in near-TIR, so the beam transmitted into the imaging media and propagated nearly parallel to the surface. The illumination intensity was 200 W/cm^2

(neglecting beam intensification by refraction at the imaging buffer/COC substrate). Fluorescence was imaged at 2.7× magnification onto an sCMOS camera (Hamamatsu ORCA-Flash 4.0 V2) through a near-infrared emission filter (Semrock #FF02-736/128) and data was collected at a 1 kHz frame rate. The FOV for 1 kHz recording was 0.39 mm x 3.9 mm (800 x 80 pixels in 2 x 2 binning).

Confocal imaging of QuasAr6a and QuaAr6b expressed in cultured rat hippocampal neuron

To sparsely expression QuasAr6b-Citrine or QuasAr6b-Citrine, rat hippocampal neuron cultures were transfected with Fsyn plasmids (HT111, HT114) encoding the constructs via Ca-Phos. Before imaging, the medium was replaced with transparent XC buffer. The confocal images were acquired on LSM880 Airyscan with an air 20× objective. Citrine fluorescence was excited with 488-nm laser.

Characterization of QuasAr6a and QuasAr6b in brain slice

Voltage imaging in acute slice

The imaging set-up was originally described in [15] with a few modifications. For the red laser path, the 639 nm laser source (CNI Lasers, MLL-FN-639, l = 639 nm, 1 W single transverse mode) was attenuated with a half-wave plate and polarizing beam splitter and directed to the center of the FOV. The size of the beam was adjusted to be slightly larger than the size of a typical neuron soma. The blue laser path included a laser source, the blue laser (Coherent, OBIs, l = 488 nm, 60 mW), an acousto-optic tunable filter (AOTF; Gooch and Housego TF525-250-6-3-GH18A) for modulating the laser intensity, and a digital micromirror device with a resolution of 1024×768 pixels (Vialux, V-7000 UV, 9515)). The waveforms of optogenetic stimulation sequence and voltage imaging sequencing were controlled via a National Instruments DAQ (NI PCIe-6363). The movies were acquired at 996.3 Hz (1 kHz) with a sCMOS camera (Hamamatsu ORCA-Flash 4.0). A Cy5 emission filter was used in the Arch-channel. The camera's internal 100 kHz clock was used as the master clock to synchronize all the DAQ inputs and outputs. The system was controlled with a custom software developed in Matlab. This Matlab-based control software includes modules interfaced with 1) the sCMOS camera, 2) DAQ; 3) DMD; 4) amplifier. Imaging was performed with a 25× water immersion objective (Olympus XLPLN25XSVMP2) with a 4-mm working distance and a numerical aperture of 1.0.

In vivo all-optical electrophysiology

Cranial window surgery for imaging visual cortical L1

For experiments in Fig. 4a-e, the window was comprised of two 3-mm round #1 cover glasses and one 5-mm round #1 cover glass (Harvard apparatus) cured together with UV curable adhesive (Norland Products, NOA 81). For experiments in Fig. 4f-i, one 3-mm round #1 cover glass was glued to a custom-made stainless-steel adapter. The adapter has an outer diameter of 5 mm and inner diameter of 2.7 mm.

The cranial window surgery for imaging L1 was performed as described previously [23]. In brief, 10 - 16 weeks-old NDNF-Cre^{+/-} mice (male or female) were induced with > 2% isoflurane and maintained in deep anesthesia with 1% isoflurane throughout the surgery. A heating pad (WPI, ATC2000) was placed beneath the mice to main the body temperature at 36 - 37 °C. Ophthalmic eye ointment was applied on the eyes to keep them moist. An approx. 3-mm craniotomy was created on the left visual cortof the exposed skull (AP: 2.5 - 2.6-mm lateral, 0.8-mm anterior of lambda) with a dental drill. The Optopatch virus was diluted to a final titer of 1×10^{13} GC/mL for experiments in cortical NDNF neurons, or to a final titer of 0.5 - 1.0×10^{13} GC/mL for experiments in hippocampal PV neurons. The diluted virus was injected at 7 - 8 sites across the craniotomy (80 and 160 µm beneath dura; 40 - 60 nL each depth; 30 - 60 nL/min). After virus injection, the craniotomy was covered with the glass window. The edge of the window was glued to the skull with cyanoacrylate adhesive (3M Vetbond). Next, a titanium headplate (designed based on [23]) was attached to the exposed skull with dental cement (C&B metabond, Parkell, No. 242-3200). Special care was taken to ensure that the dental cement filled the space between the rim of the window and the skull and covered all the exposed area of the skull. Animal typically recover from anesthesia within 20 min. Then they were returned to their home cage and administrated with Carprofen (5 mg/kg) and Buprenorphine (0.1 mg/kg) on post-surgery Day 0, 1, 2.

Window surgery for imaging hippocampus CA1

The window surgery for imaging hippocampus CA1 was performed based on previous reports [15, 24]. In brief, the cannula window was comprised of a 1.5-mm segment of a 3-mm outer diameter thin-walled stainless steel tube (MicroGroup) and 3 mm #1 round cover glass (Harvard Apparatus) glued to one end of the tube using UV-curable adhesive (Norland Products, NOA 81). 8 - 12 weeks old PV-Cre^{+/-} mice (male or female) were used for imaging. A 3-mm craniotomy was created on the left hemisphere (1.8 mm lateral, 2.0 mm caudal of bregma) with a biopsy punch (Miltex). Optopatch virus was diluted to 2.5 ~ 5 $\times10^{12}$ GC/mL and injected into three sites near the center of the craniotomy (1.0 mm to 1.4 mm beneath dura with 0.1 mm increment; 40 nL each depth; 60 nL/min). After virus injection, the cortwas carefully aspirated, and the center region of the external capsule was removed to expose the hippocampus CA1. The cannula was then

lowered onto the CA1 surface until the window touched the tissue. The remaining outer surface of the cannula was sealed to the exposed skull with dental cement (C&B Metabond). Finally, a titanium head plate was fixed onto the exposed skull. The post-surgery care was identical to that of the cranial window surgery for L1 imaging.

Optical systems for in vivo all-optical electrophysiology

The imaging set-up was originally described in [3] with a few modifications. For the red laser path, the 639 nm laser source (CNI Lasers, MRL-FN-639, l = 639 nm, 700 mW single transverse mode, later replaced by a Coherent OBIS, l = 637 nm 140mW Laser) was attenuated with a half-wave plate and polarizing beam splitter, expanded to a collimated beam of ~10 mm diameter, then projected onto the surface of a reflection-mode liquid crystal spatial light modulator (SLM, Meadowlark 1920SLM VIS) with a resolution of 1920×1152 pixels. For the blue laser path, the blue laser (Coherent OBIS, l = 488 nm, 100 mW) was modulated in intensity via an acousto-optic tunable filter (AOTF; Gooch and Housego TF525-250-6-3-GH18A) and collimated to a beam of ~17 mm in diameter before being directed onto the reflective surface of a digital micromirror device with a resolution of 1024×768 pixels (DMD, Vialux, V-7001 VIS). The waveforms of optogenetic stimulation sequence and voltage imaging sequencing were controlled via a National Instruments DAQ (NI PCIe-6363). The movies were acquired at 1,000 - 4,000 Hz with a sCMOS camera (Hamamatsu ORCA-Flash 4.0). A Cy5 emission filter was used in the Arch-channel. The camera's internal 100 kHz clock was used as the master clock to synchronize all the DAQ inputs and outputs. The system was controlled with a custom software developed in Matlab. This Matlab-based control software includes modules interfaced with 1) the sCMOS camera, 2) DAQ; 3) DMD, and 4) SLM. The software also includes routines for registration of SLM, DMD and camera.

Data analysis

Data were analyzed and plotted with homemade code written in MATLAB.

Extracting the voltage-sensitive fluorescence from in vitro and ex vivo imaging

We used a previously described maximum-likelihood pixel-weighting algorithm [25] to define the mask for voltage-sensitive fluorescence. Whole-cell masks were initially manually defined. Then the raw whole-cell fluorescence from the cell masks was used to guide the algorithm to automatically find the pixels carrying the most information. Based on the weighting information, new masks excluding the least informative pixels were created. Then the pixel-selective masks were applied to the original movie to calculate fluorescence from the unweighted mean of pixel

values within the selected ROIs. For GEVIs like QuasAr6 with good trafficking, we often found that the pixel-selective masks correspond to the cell membranes. For calculations of Δ*F*/*F* in HEK293T and neuron culture, fluorescence from a cell-free region was deemed as the baseline signal of the cell and extracted from each trace.

In our experiences, the value of Δ*F*/*F* is highly variable in tissue slice and live brain, where multiple factors such as the depth of the cell, light scattering, the intensity of autofluorescence, and patterned illumination, may affect baseline determination. Thus, for voltage imaging in slice and in the brain, we mostly used either signal-to-noise ratio (SNR) or relative signal normalized to the full spike height to represent the voltage-sensitive fluorescence change. In Fig. 3m, p, no baseline correction was applied, and the Δ*F*/*F* in these plots are not accurate measurements of the *V-F* relationship.

Extracting the voltage-sensitive fluorescence from in vivo imaging

Movies were corrected for motion using the NoRMCorre algorithm [1]. Next, photobleaching was corrected using mono-exponential fit. Next, masks for each cell were manually defined, and the movie was divided into sub-movies based on the contour of the cell masks. To accurately extract the subthreshold dynamics, we performed activity-based image segmentation separately in each sub-movie. Our assumption was that while subthreshold voltages could be correlated between a cell and out-of-focus background cells, spike dynamics are unlikely to be correlated with background. We also assumed that spiking dynamics and the true subthreshold dynamics would share the same spatial footprint. The sub-movies were filtered in time with a 50 Hz high-pass filter, and then segmented semi-automatically using principal components analysis followed by time-domain independent components analysis (PCA/ICA). The spatial masks from PCA/ICA were then applied to the original movies without high-pass filtering to extract fluorescence traces that included both spike and subthreshold dynamics.

We found that the quality of the spatial masks generated by PCA/ICA depended on the SNR of the raw movie, as well as the number of spikes in the raw movie. In general, the stronger SNR in the raw movie, and the more spikes in the segmented epoch, the more likely we obtain high-quality spatial masks. For some recordings where the SNR was good enough for accurate detection of spikes (SNR > 4), but did not give high-quality PCA/ICA masks, these recordings were only used to analyze spike dynamics, but not for extracting subthreshold dynamics. Because PCA/ICA is biased towards high-SNR recordings, in Fig. 4 and Extended Data Fig. 8 where the *in vivo* SNR were compared, we used the manually-created mask to extract the fluorescence trace.

Spike detection and trace normalization

Fluorescence traces were first high-pass filtered (medfilt1, window = 25 ms unless otherwise indicated). We used two complementary methods for spike detection. First, a simple threshold-and-maximum procedure was applied on the high-pass filtered fluorescence trace. The initial threshold was set at 3 times of the noise level and adjusted if necessary. Second, we performed wavelet transformation on the high-passed filtered traces to extract the signals based on the time-domain (Matlab Wavelet toolbox). Specifically, we performed the maximal overlap discrete wavelet transform (modwt, wavelet type = ''sym4', computed to level 8). We next projected the higher-frequency wavelets (level 2, 3, 4) into a time trace (imodwt,'sym4'), then applied a threshold-and-maximum procedure to identify the peaks in the projected traces Compared to Fourier transformation, wavelet decomposition allows the expansion of signals in terms of finite time functions, which gives higher selectivity to impulse-like events such as action potentials. A fluorescence impulse was accepted as spikes only if it stood out in both spike detection methods. We found the wavelet transformation particularly helpful to spike detection in PV neurons because PV neurons' characteristically narrow spikes were much faster than most sources of noises. All fluorescence traces were then normalized to spike height for spike triggered average.

Calculation of spike SNRs and waveforms

We define SNR as the ratio of the height of spike (fluorescence signal above the subthreshold) to the high-frequency noise. The high-frequency noise was defined as the standard deviation of the non-spiking epoch of the high-pass filtered (medfilt1, window = 25 ms) fluorescence trace. Because the intensity of photocurrent modulated the height and waveform of the spike, we only used the ramp epoch to calculate spike height and waveforms. For PV spikes, we used all the spikes from the upward- and downward- ramps. For the NDNF spikes, because the ramp of the blue light was steeper, we found the spike height and waveform varied quickly. Thus, we only used the first three spikes from the ramp for the calculation.

Estimation of spike rate with Bayesian Adaptive Kernel Smoother

In the double Optopatch experiments on the NDNF+ cells, the duration of the stimulation was short so the total number of the spikes were limited. As a result, the calculation of the spike rate was sensitive to the choice of integration window. Thus, we used a Bayesian Adaptive Kernel Smoother (BAKS) [26] to convert discrete spike raster into continuously varying spike rate. The Matlab function was downloaded from https://github.com/nurahmadi/BAKS. The shape parameter (a) and the scale parameter (b) were both set to 40. As a quality control, we compared the average

of the BAKS-derived spike rate against the average spike rate directly calculated from the spike raster. We found the two methods in good agreement.

Test for bias for or against reciprocal connections

Consider measurements on N cell pairs (N = 22 in our data), which yield n_2 reciprocally connected pairs (n_2 = 8), n_1 unidirectionally connected pairs (n_1 = 10), and n_0 unconnected pairs (n_0 = 4). We have $n_0 + n_1 + n_2 = N$ and the total number of directed connections is $M = 2n_2 + n_1$. In our dataset, M = 26.

The number of ways of selecting n_1 single and n_2 double connections is:

$$\Gamma(n_1, n_2) = \binom{N}{n_2}\binom{N - n_2}{n_1} 2^{n_1} ,$$

where $\binom{X}{Y} = \frac{X!}{Y!(X-Y)!}$.

This expression simplifies to:

$$\Gamma(n_1, n_2) = \frac{N!}{n_2!n_1!n_0!} 2^{n_1}.$$

The total number of ways of arranging the M connections among the N cell pairs is

$$\Gamma_{tot} = \binom{2N}{M}.$$

Under the null hypothesis that connections are distributed independently, then the probability of observing n_2 reciprocal and n_1 unidirectional connections, given M total connections, is:

$$P_M(n_1, n_2) = \frac{\Gamma(n_1,n_2)}{\Gamma_{tot}}.$$

The probability distribution $P_{26}(n_1, n_2)$ is maximal at n_1 = 10 and n_2 = 8, which are precisely the numbers we measured.

Estimate of optical crosstalk between PV pairs

We reasoned that the upper limit of optical crosstalk between cell pairs could be estimated using the fluorescence signal extracted from an intervening mask midway between the two cells. The intervening mask was created as follows. First, the area and centroid of the cell masks was determined with Matlab function regionprops. Second, a circular mask was created, with its center coordinates at the mid-point between the centroids of the two cell masks, and its area set to be the sum of the areas of both cell masks. However, when the cells were too close, the intervening mask may overlap with the cell mask. Thus, the pixels located within the circular mask radius from the cell mask centroid were removed from the middle mask. The resulting masks generally had comparable, or larger size than the cell masks. The fluorescence signal was extracted by applying the intervening mask to the motion-corrected movie, corrected for any photobleaching and high-pass filtered, and normalized with the voltage fluorescence traces. The optical crosstalk was

calculated as the average fluorescence waveform triggered by the same set of spikes used in calculating cross-triggered average.

Quantifying the gap junction-induced spikelet

The spike-triggered voltage waveform (STVW) was calculated using the PCA/ICA extracted fluorescence trace. For the cross spike-triggered voltage waveform (STVW), only events where only one cell spiked (spike peaks in the two cells separated by > 10 ms) were included in the analysis to avoid spurious contributions to a short-time peak from near-coincident spikes. The same set of spikes were used to calculate the self-STVW. The cross-STVW were then normalized with the height of the post-synaptic self-STVW. In Fig. 6c, to preserve the low subthreshold coupling, the fluorescence trace was high-passed filtered with a window of 25 ms. In the double Optopatch experiment in PV cells where the aim was to analyze the fast optogenetically evoked coupling, the fluorescence traces were high-pass filtered with a smaller window of 8 ms. The self- and cross-STVW were calculated over the window from -100 ms to 100 ms (401 data points). The height of the spikelet was determined from the normalized signal at $t = 0$. The p-value was calculated as follows. First, an empirical null distribution was computed using the STA measurements at times $t \neq 0$ (n = 400 time-points). This distribution reported fluctuations due to noise. Next, a p-value for the STA measurement at time $t = 0$ was computed as $p = r / n$, where r is the rank of the STA measurement at time $t = 0$ (higher values correspond to lower ranks), and n is the number of STA measurements. This p-value corresponds to the null hypothesis that the STA measurements at $t \neq 0$ are greater than or equal to the STA measurements at $t = 0$. Spikelets are defined as those events with $p < 0.05$ and amplitudes > 2% of the action potential amplitude.

REFERENCES

1.   Pnevmatikakis, E.A. & Giovannucci, A. NoRMCorre: An online algorithm for piecewise rigid motion correction of calcium imaging data. *J Neurosci. Methods* **291**, 83-94 (2017).
2.   Werley, C.A., Chien, M.P. & Cohen, A.E. Ultrawidefield microscope for high-speed fluorescence imaging and targeted optogenetic stimulation. *Biomed. Opt. Express* **8**, 5794-5813 (2017).
3.   Fan, L.Z. et al. All-Optical Electrophysiology Reveals the Role of Lateral Inhibition in Sensory Processing in Cortical Layer 1. *Cell* **180**, 521-535 e518 (2020).
4.   Chien, M.P. et al. Photoactivated voltage imaging in tissue with an archaerhodopsin-derived reporter. *Sci. Adv.* **7**, eabe3216 (2021).
5.   Piatkevich, K.D. et al. Population imaging of neural activity in awake behaving mice. *Nature* **574**, 413-417 (2019).
6.   Fan, L.Z. et al. All-optical synaptic electrophysiology probes mechanism of ketamine-induced disinhibition. *Nat. Methods* **15**, 823-831 (2018).

7.   Hochbaum, D.R. et al. All-optical electrophysiology in mammalian neurons using engineered microbial rhodopsins. *Nat. Methods* **11**, 825-833 (2014).
8.   Nguyen, C. et al. Simultaneous voltage and calcium imaging and optogenetic stimulation with high sensitivity and a wide field of view. *Biomed. Opt. Express* **10**, 789-806 (2019).
9.   Kimura, T. et al. Production of adeno-associated virus vectors for in vitro and in vivo applications. *Sci. Rep.* **9**, 13601 (2019).
10.   Zhang, H., Reichert, E. & Cohen, A.E. Optical electrophysiology for probing function and pharmacology of voltage-gated ion channels. *eLife* **5**, e15202 (2016).
11.   Huang, Y.L., Walker, A.S. & Miller, E.W. A Photostable Silicon Rhodamine Platform for Optical Voltage Sensing. *J. Am. Chem. Soc.* **137**, 10767-10776 (2015).
12.   Paez-Segala, M.G. et al. Fixation-resistant photoactivatable fluorescent proteins for CLEM. *Nat. Methods* **12**, 215-218 (2015).
13.   Subach, F.V. et al. Photoactivatable mCherry for high-resolution two-color fluorescence microscopy. *Nat. Methods* **6**, 153-159 (2009).
14.   Patterson, G.H. & Lippincott-Schwartz, J. A photoactivatable GFP for selective photolabeling of proteins and cells. *Science* **297**, 1873-1877 (2002).
15.   Adam, Y. et al. Voltage imaging and optogenetics reveal behaviour-dependent changes in hippocampal dynamics. *Nature* **569**, 413-417 (2019).
16.   Kim, J.H. et al. High cleavage efficiency of a 2A peptide derived from porcine teschovirus-1 in human cell lines, zebrafish and mice. *PLoS One* **6**, e18556 (2011).
17.   Piatkevich, K.D. et al. A robotic multidimensional directed evolution approach applied to fluorescent voltage reporters. *Nat. Chem. Biol.* **14**, 352-360 (2018).
18.   Bolger, A.M., Lohse, M. & Usadel, B. Trimmomatic: a flexible trimmer for Illumina sequence data. *Bioinformatics* **30**, 2114-2120 (2014).
19.   Gaspar, J.M. NGmerge: merging paired-end reads via novel empirically-derived models of sequencing errors. *BMC Bioinformatics* **19**, 536 (2018).
20.   Li, H. & Durbin, R. Fast and accurate short read alignment with Burrows-Wheeler transform. *Bioinformatics* **25**, 1754-1760 (2009).
21.   Li, H. et al. The Sequence Alignment/Map format and SAMtools. *Bioinformatics* **25**, 2078-2079 (2009).
22.   Walker, B.J. et al. Pilon: an integrated tool for comprehensive microbial variant detection and genome assembly improvement. *PLoS One* **9**, e112963 (2014).
23.   Goldey, G.J. et al. Removable cranial windows for long-term imaging in awake mice. *Nat. Protoc.* **9**, 2515-2538 (2014).
24.   Dombeck, D.A., Harvey, C.D., Tian, L., Looger, L.L. & Tank, D.W. Functional imaging of hippocampal place cells at cellular resolution during virtual navigation. *Nat. Neurosci.* **13**, 1433-1440 (2010).
25.   Kralj, J.M., Douglass, A.D., Hochbaum, D.R., Maclaurin, D. & Cohen, A.E. Optical recording of action potentials in mammalian neurons using a microbial rhodopsin. *Nat. Methods* **9**, 90-U130 (2012).
26.   Ahmadi, N., Constandinou, T.G. & Bouganis, C.S. Estimation of neuronal firing rate using Bayesian Adaptive Kernel Smoother (BAKS). *Plos One* **13**, e0206794 (2018).